scientific reports

Check for updates

OPEN

Detection of H_2S, HF and H_2 pollutant gases on the surface of penta-$PdAs_2$ monolayer using DFT approach

Dhara Raval[1], Sanjeev K. Gupta[2]✉ & P. N. Gajjar[1]✉

In this research, the adsorption of targeted noxious gases like H_2S, HF and H_2 on penta-$PdAs_2$ monolayer are deeply studied by means of the density functional theory (DFT). After the capturing of three kind of pollutant gases (H_2S, HF and H_2), it is observed that, the electronic properties are slightly affected from the pristine one. In all cases, the physisorption interaction found with adsorption energy of − 0.49, − 0.39 and − 0.16 eV for H_2S, HF and H_2 gases, respectively. Which is exposed that H_2S gas strongly absorbed on penta-$PdAs_2$ nanosheet. In case of HF (H_2) gas adsorbed systems, the obtained charge transfer is + 0.111 e (+ 0.037 e), revealed that the electrons are going to $PdAs_2$ nanosheet from the HF (H_2) molecules. Further, under the non-equilibrium Green's function (NEGF) theory, the IV response and sensitivity of absorbed H_2S, HF and H_2 have been discussed. The results demonstrate that the H_2S molecules on $PdAs_2$ has suitable adsorption strength and explicit charge transfer compared with other targeted molecules. Hence, our novel findings of H_2S, HF and H_2 targeted gas sensing on penta-$PdAs_2$ nanosheet might provide reference-line to design modern gas sensor device at the nano-scale.

H_2S, HF and H_2 are toxic and colorless gases, and they are common industrial and environmental pollutants, and also became extensive range sources of health effects[1–3]. Additionally, due to rapid industrialization, universally use of chemicals, transportation of automobiles has led to increasing global environmental pollution and diminution of the ozone layer, which has expected a great hazard and major threat to the human health[4–6]. However, the arena of gas sensing has always concentrated on the research in control of environmental pollution, monitoring of industrial activities, health diagnostics and noxious gas sensing's sake of public safety[7–9]. In recent years, numerous nanomaterials have been scrutinized for gas sensing applications. In spotlight, the two-dimensional (2D) nanomaterials have castoff to sense a low concentration of gas molecules in sensing applications because of their compensations like, high stability, novel structures, large surface area/volume ratio, excellent adsorption abilities and low cost[10–19]. For example, graphene[20], Phosphorene[21], carbon nitride compound[22], B_4C_3 monolayer[23], InN monolayer[24] and transition-metal dichalcogenides (TMDs) like $MoSe_2$, $PtSe_2$, SnS_2 and HfS_2, etc.[25–30], have become the burgeoning materials as toxic gases sensor.

Moreover, the key foundations of (i) H_2S gas are from volcanic gas, fuel, sewage plants, sulfur deposits and ammonia synthesis from hydrocarbon feedstock[31–37]. Although, very recently, a study shows B_4C_3 nanosheet, as excellent gas sensor for CO, NO, NH_3, SO_2 and H_2S[23] and Gao et al.[38], testified the strong adsorption capacity of H_2S and CH_4 with the modified 2D graphene sheet. Then, (ii) HF gas is also eminent toxic gas it is mainly originate from industrial processes at high temperature and the combustion of products containing fluoride, which is harmfully affect to not even only human but also flora and fauna. The high exposure of HF gas causes, muscle spasms and result may even in fatality at extreme cases[2].

Bhattacharya et al.[38], also studied the sensing of HF, HCN and H_2S with nitrogenated holey carbon (C_2N-*h*2D) monolayer. Next, (iii) H_2 a tasteless, odourless and flammable gas. Even, by lacking O_2 concentration in enclosed area, only 4% concentration of H_2 gas could be reasons to burnt and suffocation[39]. Li et al.[40] also explored Ru-doped $PtSe_2$ monolayer as good sensor of H_2 gas and Pandey et al.[41] also suggested that MoS/WS monolayer is potential substrates for gas sensing of H_2, NO and CO gases.

[1]Department of Physics, University School of Sciences, Gujarat University, Ahmedabad 380009, India. [2]Computational Materials and Nanoscience Group, Department of Physics and Electronics, St. Xavier's College, Ahmedabad 380009, India. ✉email: sanjeev.gupta@sxca.edu.in; pngajjar@gujaratuniversity.ac.in

Apart from aforementioned two-dimensional (2D) materials gas sensor, the newly discovered pentagonal structures had been also showed to design gas sensor due to its superior quality such as high surface carrier mobility, large surface area, more adsorption sites and great optical properties over the traditional unit hexagon structure[42,43]. Additionally, in past, several 2D pentagon unit structure has also been reported for the promising candidates for innovative applications in the gas sensor. Like, Wei et al.[44] predicted that penta-BCN monolayer is good sensor of CO, H_2S, NH_3 and NO gas molecules and stated that the targeted gases have moderate adsorption energies in the range of − 0.797 eV to − 1.186 eV and proved it as potential applicant for said gas molecules sensors applications. Lakhani et al.[45] shows the dissociation of air pollutants on the uniform surface of pentagonal BeP_2 monolayer using first principles study. Xia et al.[46] also explored that penta-$PdSe_2$ monolayer has meaningful and promising material to be applied in FET type gas sensors as detection of NO_2 gas. Then, Tang et al.[47] revealed the new sensor material P-SiC_2 monolayer and concluded that after the contact with NO_2 gas the electronic resistance of P-SiC_2 monolayer is decreased significantly, which indicating the ultrahigh sensitivity towards NO_2 sensing. Hereafter, inspired by these Penta two-dimensional (2D) gas sensing research work owing to their robust adsorption capabilities and sensitivity, herein we are first time examined H_2S, HF and H_2 gas sensing capabilities on the newly discovered novel penta-$PdAs_2$ monolayer, because modelling new gas sensing resources have paramount bid to probe the pollutant molecules in the current era. Viz, H_2S, HF and H_2 gases. And finding an effective material to detecting and adsorbing these toxic (H_2S and HF) and highly flammable (H_2) gases are great worth to protect our living environment for modern civilization. Even though, the outstanding electronic properties, transport, and optical properties of pristine penta-$PdAs_2$ monolayer is previously done by our research group[48].

In this work, the capacity of monolayer penta-$PdAs_2$ as gas sensor (of H_2S, HF and H_2 gases) capture is discovered by first-principles calculations. As density functional theory calculation is a widespread and feasible approach for simulation of gas adsorption on the novel nano-surfaces. Henceforth, the adsorption process of H_2S, HF and H_2 gases on penta-$PdAs_2$ monolayer was studied and compared by evaluating differences in adsorption energy (E_{ad}), appearance change (e), charge transfer (Q), work function (Φ), charge density difference (CDD), electronic band structure, density of states/eV (DOS) and partial density of states/eV (PDOS) in this research note. These observations deliver quest of sensor materials with high sensitivity and selectivity towards pollutant gases such like H_2S, HF and H_2.

Simulation details

Density Functional theory (DFT) calculations were executed using SIESTA code[49] to examine the optimization, electronic and adsorption (of targeted gases) properties of penta-$PdAs_2$ nanosheet. To treat the exchange–correlation (XC) effect, the generalized gradient approximation (GGA) of the Perdew–Burke–Ernzerhof (PBE)[50] functional was employed. We incorporated the *DRSLL* dispersion correction method to treat the long range *vdWs* forces[51]. The Kohn–Sham one electron states were expanded in a plane-wave basis set. The plane wave kinetic energy cut-off is considered as 450 Ry. The doubled zeta plus (*DZP*) basis set was used with an energy of 0.01 Ry to expand the Kohn–Sham orbital. The Brillouin zone sampled using a $5\times5\times1$ Monkhorst–Pack k-point mesh during structural optimization[52]. The **k**-point mesh was then increased to $15\times15\times1$ to attain more accurate results for electronic structure simulations. The optimized structures of $3\times3\times1$ supercell penta-$PdAs_2$ monolayer is shown in Fig. 1a. As aforementioned, potential properties of penta-$PdAs_2$ monolayer such as structural, electronic, transport and optical properties have already reported by our group[48] and proven that it is dynamically stable via the positive phonon frequencies of penta-$PdAs_2$. Hence, using same substrate of penta-$PdAs_2$, herein we reported the sensing potential in the penta-$PdAs_2$ monolayer for H_2S, HF and H_2 gases. All the optimized structures were relaxed without given any geometric constraint (GC) on the sheet. The atomic force is specified as 0.01 eV/Å to relaxing the systems. A vacuum of 15 Å have been considered along the perpendicular direction of the penta-$PdAs_2$ surface to avoid the interaction of periodic boundary conditions as employed in XY-plane. The adsorption energy is determined by the following equation[53]:

$$E_{ads} = E_{\text{nanosheet+Gas}} - E_{\text{nanosheet}} - E_{\text{Gas}}, \tag{1}$$

where, $E_{\text{nanosheet+Gas}}$ represents the total energy of the penta-$PdAs_2$ nanosheet with the gas molecules absorbed on, while $E_{\text{nanosheet}}$ and E_{Gas} are the total energy of penta-$PdAs_2$ sheet without the gas molecules and the isolated gas molecules, respectively. From the adsorption energy definition, a negative E_{ads} specifies an exothermic process and thermodynamically favourable for molecular gas sensing. All the initial distances between sheet and gas molecules are set to 2.0 Å. The Hirshfeld atomic population analysis method was used to estimate the charge transfer (Q) as defined in SIESTA and negative value of Q means that electron transfer sheet to gas molecules. The charge density difference (CDD) $\Delta\rho$ between the adsorbed and isolated gases is calculated by:

$$\Delta\rho = \rho_{\text{nanosheet+Gas}} - \rho_{\text{nanosheet}} - \rho_{\text{Gas}}, \tag{2}$$

where, $\rho_{\text{nanosheet+Gas}}$, $\rho_{\text{nanosheet}}$ and ρ_{Gas} are represent the charge densities of penta-$PdAs_2$ monolayer with, without the adsorption of gas and charge density of gas molecules, respectively. This CDD has been imagined with utility of VESTA software[54]. The recovery time (τ) is the crucial parameter for gas sensor, which can be measured experimentally ranging from second to several minutes. Based on activated-complex theory[55], recovery time has been defined by:

$$\tau = \omega^{-1}\exp\left(-\frac{E_{ads}}{K_B T}\right), \tag{3}$$

where, ω is the attempt frequency ($\sim 10^{12}$ s^{-1}), E_{ads} is adsorption energy, K_B is Boltzmann' Constant and T is temperature. At last, based on non-equilibrium *Green's* function (NEGF), the IV response was examined by

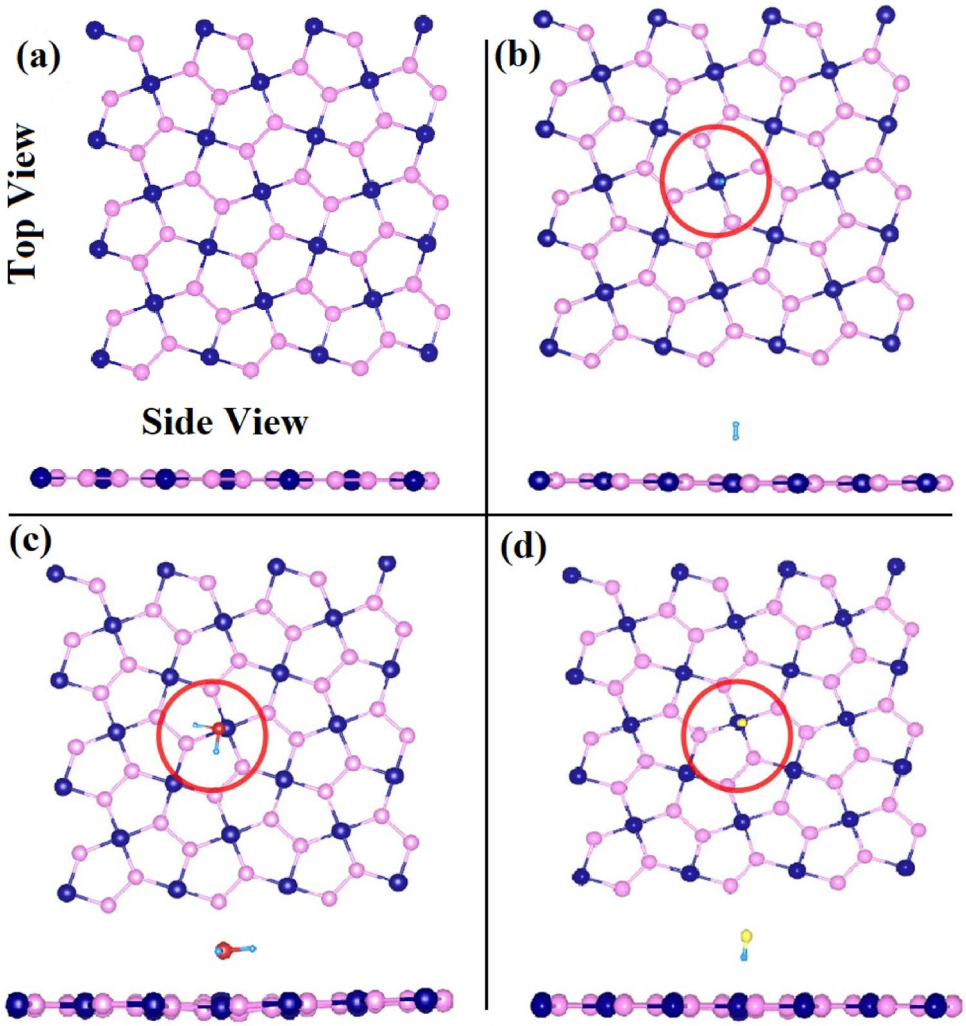

Figure 1. Side and top view of the (**a**) Bare penta-$PdAs_2$ monolayer and after gas adsorption of (**b**) H_2 (**c**) H_2S and (**d**) HF. The Pd, As, H, S and F atoms are indicated in navy blue, pink, water blue, red and yellow colors, respectively.

TRANSIESTA package[56]. The current (I) through the scattering region is calculated by exploring the Landauer-Buttiker formalism,

$$I(V_{bias}) = G_0 \int_{\mu_L}^{\mu_R} T(E, V_{bias}) \left[f(\mathrm{E} - \mu_L) - f(\mathrm{E} - \mu_R) \right] dE, \tag{4}$$

where, G_0 is quantum conductance and $T(E, V_b)$ is the transmission probability of an electron incident at an energy E through the device under the bias voltage V_{bias}, μ_L and μ_R are the electrostatic potentials of left and right electrodes.

Results and discussions

Adsorption of H_2, H_2S and HF gases on penta-$PdAs_2$ monolayer. In the first step, we have systematically examined the geometries of pristine penta-$PdAs_2$ monolayer. The optimized structure of penta-$PdAs_2$ is displayed in Fig. 1a. The bond length between Pd–As and As–As are 2.51 Å and 2.32 Å, respectively, which are comparable with previous reported studies[57]. To study the electronic properties such as the electronic band structure, DOS and PDOS were calculated and the obtained electronic band gap (E_g) of penta-$PdAs_2$ is 0.34 eV[48]. In the second step, we have optimized the gas molecules of H_2S, HF and H_2 on the surface of penta-$PdAs_2$ sheet. We have placed the gas molecules at all possible parking sites on the sheet and initially molecules are fixed at the (i) Hollow (ii) Top of Pd atom (iii) Top of As atom (iv) Bridge of Pd-As and (v) Bridge of As-As atoms. The adsorption energy of each case is reported in ESI (Table S1, ESI) and highest adsorption energy site is considered for the further calculations. Therefore, the most favorable sites of H_2S and H_2 gases are perceived at bridge of Pd-As with adsorption distance of 2.91 Å and 2.70 Å, respectively. While HF gas is relaxed on the top of Pd atom with distance of 2.34 Å. Although, after the relaxation of that sites, the gas molecules are shifted on the top of Pd atom in all cases, which is shown in Fig. 1b–d. After the stable adsorption, the bond length between H–S, H–H,

and H–F are 1.37, 0.77 and 0.94 Å, respectively and the bond angle of non-linear H_2S is 92.142°, which is agreed with previous reported work[58].

Table 1 presents the adsorption energy (E_{ads}), adsorption distance (d) and relaxation time (τ) and type of interaction for considered H_2S, HF and H_2 gas molecules on the surface of penta-$PdAs_2$ monolayer. As shown in table, the calculated adsorption energy of H_2S, HF and H_2 gases are − 0.49, − 0.39 and − 0.16 eV, respectively. The E_{ads} values of H_2S, HF and H_2 were negative, suggesting that the adsorption process was all energetically favorable on the penta-$PdAs_2$ monolayer and all in the physisorption range. Among three gases, H_2S (HF) has strongest with 0.49 (0.39) eV compared to H_2, it has the weakest adsorption strength about $E_{ads} \sim 0.16$ eV. Although, the obtained adsorption energy of H_2 is 18.75% higher compared to adsorbed on phosphorene (0.13 eV) nanosheet[59]. Additionally, Majidi et al. reported the HF and H_2S detection on the twin graphene and Ti-embedded twin graphene with quoted adsorption energy of − 0.16 and − 0.22, respectively[58]. Which means, present results are quite good compared to them as H_2S and HF gas sensor on penta-$PdAs_2$ sheet. On other side, the obtained adsorption energy of H_2S gas on penta-$PdAs_2$ monolayer is − 0.49 eV, which is smaller than penta-BCN monolayer (− 0.797 eV)[44], but relatively larger than functionalized graphene[58] and phosphorene (− 0.41 eV)[21]. Further, it also be noted that the recovery time (τ) plays a crucial role in sensing application, τ is also summarized in the Table 1. The obtained sequence of the recovery time (τ) for three gases are as follow: $H_2 < HF < H_2S$. Although, the recovery time of H_2S is very long owing to the strong adsorption capacity of $PdAs_2 + H_2S$ (0.49 eV). Hence, the low value of recovery time strongly specified that $PdAs_2 + H_2S$ configuration have high selectivity and can be good choice as reversible sensors of H_2S.

Moreover, the charge transfer mechanism was studied by Hirshfeld atomic population analysis and results are summarized in Table 2. The value of $Q < 0$ indicates that H_2S (− 0.137 e) gas molecules accept the electrons from the $PdAs_2$ sheet. whereas $Q > 0$, in HF (+ 0.111) and H_2 (+ 0.037) indicates that both gas molecules are donating electrons to the $PdAs_2$ sheet as result of that holes are expected to stay in the gas molecules as depicted in Fig. 2 by the blue arrow. Figure 2a–c, shows the charge density difference ($\Delta\rho$), which is obtained by the Eq. (2). From that, it can be observed that, charge is accumulated at the negative charge region (shown as green color) and charge is depleted in the positive charge region (shown as orange color) due to the reformed of the effective interface dipoles and polarization of electrons. Where adsorption energy (E_{ads}) is taking place to form the redistribution of electrons at the interface region. Here, among the three gases, the H_2S has higher charge transfer between the adsorbing $PdAs_2$ sheet suggesting that H_2S has effective and strong detection with high selectivity towards the penta-$PdAs_2$ nanosheet compared to the HF and H_2 gases.

The surface sensitivity of the 2D nanosheet could also approached by determining the differences in work function parameter (Φ)[60] as illustrate:

$$\Phi = V_{\infty} - E_F, \tag{5}$$

where, V_{∞} and E_F are the electrostatic potential and the fermi energy level, respectively. Basically, the work function describes the minimum energy needed to dislodge an electron from the surface of penta-$PdAs_2$ monolayer. The calculated work function of penta-$PdAs_2$ with H_2S, HF and H_2 lies in the range of 4.63 to 4.70 eV, as tabulated in Table 2 and electrostatic potential energy level is presented in in Fig. 3a–d. The red and black dashed line indicates the fermi energy level (E_F) and energy vacuum level (V_{∞}), respectively and the black double head arrow gives the work function values. The value of Φ of bare graphene is 4.5 eV which shows it as an ideal material for where work function optimization is vital[61]. As shown in Table 2, the Φ of bare penta-$PdAs_2$ monolayer is 4.63 eV that is slightly larger than the graphene[61]. The nature of the Φ is symmetric for H_2S, HF and H_2 gas molecules with Φ value of 4.573 eV, 4.708 eV and 4.634 eV, respetively. Because of the adsorption of gases, the Φ is increase in all the cases compared to bare $PdAs_2$ monolayer demonstrating that the electrons are transferring to the vacuum level is obstructed. Therefore, the Φ can be effectively affected by the adsorption of H_2S, HF and

System	E_{ads} (in eV)	d (Å)	τ (in μs)	Interaction type
$PdAs_2$	–	–	–	–
$PdAs_2 + H_2$	− 0.16	2.70	0.00053	Physisorption
$PdAs_2 + H_2S$	− 0.49	2.91	179	Physisorption
$PdAs_2 + HF$	− 0.39	2.34	4.24	Physisorption

Table 1. The adsorption energy (E_{ads}), adsorption distance (d), relaxation time (τ) and interaction type.

System	E_g (eV)	Q (e)	Φ (eV)	Style
$PdAs_2$	0.34	–	4.631	–
$PdAs_2 + H_2$	0.30	+ 0.037 e	4.634	Donor
$PdAs_2 + H_2S$	0.28	− 0.134 e	4.573	Acceptor
$PdAs_2 + HF$	0.30	+ 0.111 e	4.708	Donor

Table 2. The electronic band gap (E_g), charge transfer (Q), work function (Φ) and style.

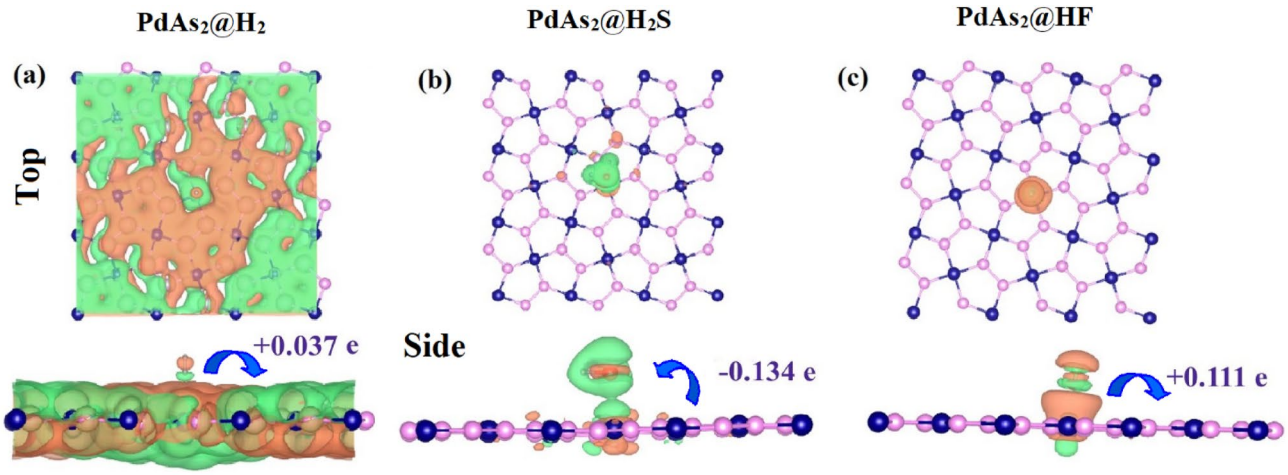

Figure 2. The charge density difference (CDD) and charge transfer of (**a**) H_2, (**b**) H_2S and (**c**) HF molecules after absorbed. Green and orange color represent accumulation and depletion of charge, respectively. The isovalue used for plotting is 0.03 e/Å^3.

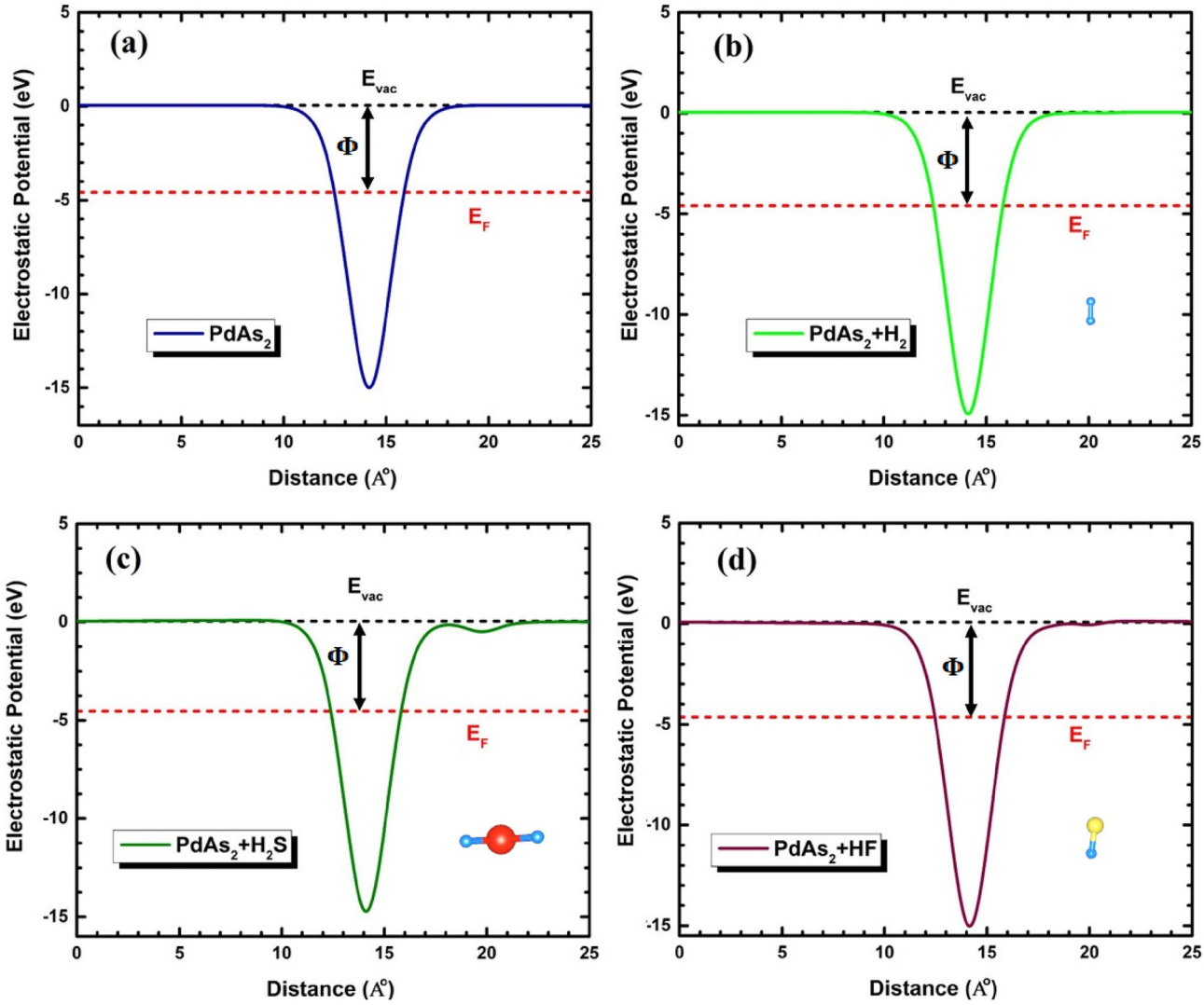

Figure 3. The planar average of the electrostatic potential of (**a**) bare monolayer and adsorbed with (**b**) H_2, (**c**) H_2S and (**d**) HF gas molecule.

H_2 gas molecules on $PdAs_2$ surface, which implies that Schottky barrier height can be adjusted by the H_2S, HF and H_2 gas molecules.

Electronic properties. In order to deeper elucidate the gas sensing behavior of penta-$PdAs_2$ monolayer towards H_2S, HF and H_2 gases, we analyzes the total density of states/eV (TDOS), projected density of states/eV (PDOS) and electronic band structure of gas molecules absorbed along that of bare $PdAs_2$ monolayer system. Figure 4a–d, shows the density of state before and after the adsorption of H_2S, HF and H_2 gases on the $PdAs_2$ surface. For comparison, the electronic band struture and TDOS and PDOS also demostrated in the ESI (Figs. S1, S2, ESI).

Visibly, it is confirmations no significant change either the electronic conduction or valence bands in the band structure after the adsorption of the gas molecules but the electronic band gap (E_g) is decreases from the bare counterparts. As tabulated in Table 2, the E_g decreases to 0.28 and 0.30 as a result of H_2S and HF(H_2) adsorption on pristine $PdAs_2$ monolayer, respectively. The trivial impact of H_2S, HF and H_2 molecules in the unoccupied states of the $PdAs_2$ monolayer above the fermi level is highly responsible to decreases the electronic band gap due to π to π* transition at S-point after the adsorption of the gases. Additionally, the valance bands (VBs) and conduction bands (CBs) have new sub-bands are outcome from the adsorption of H_2S, HF and H_2 gases on $PdAs_2$ monolayer. The presence of new sub-bands justifies the variations of the electronic energy levels due to the adsorption of three gases. Therefore, TDOS/eV and PDOS/eV in further utilized to investigate the energy levels of bare $PdAs_2$ prior and after adsorption of H_2 H_2S and HF as shown in Fig. 4a–d. It can be observe from Fig. 4a–d, the significant contribution in the DOS comes from the Pd-*d* and As-*p* orbitals with a small contribution from H, S and F atoms at the fermi level. From the DOS of the H_2 adsorption (Fig. 4b), one can see that $PdAs_2$ monolayer after adsorbing upholds the semiconducting feature with electronic band gap of 0.30 eV and H_2 gas molecules acts as electron donor. However, there is no more influence seen at fermi level between $PdAs_2 + H_2$ and bare $PdAs_2$ monolayer. But, the *1s* orbital of H atom in the H_2 is mainly hybridizied with the *4p* orbital of the As atom and localized between 5 to 6 eV in the conduction bands as shown in Fig. S2a. While in case of H_2S absorption (Fig. 4c), the highest occupied molecules orbital (HOMO) was mainly dominated by the interrelation of the H-*1s* and S-*3p* orbital of the H_2S gas molecules and induces distinct states around 3.5 to 4.5 eV in the CBs. The same trend also follows in the adsorbing of H_2S gas molecules on the CoOOH sheet surface[62]. The relatively higher adsoprtion energy and charge transfer of H_2S on the $PdAs_2$ sheet surface was due to the hybridyzation between the Pd-*4d* and S-*3p* states near the fermi level in the VBs as depicted in Fig. S2b. Similarly, after the adsorption of the HF gas molecules (Fig. 4d), the energy around 4 to 6 eV is arised due to the mixing of the H-*1s* and F-*2p* orbital in the HOMO region. While strong contribution of the hybridization of the F-*2p* (− 4 to − 2 eV) orbitals and Pd-*4d* are responsible for the next higher adsorption energy of the $PdAs_2 + HF$ system and acts as the electron donor near the fermi energy level as viewed in Fig. S2c. Likewise, very recently, Kaur et al. also reported the 2D janus WSSe monolayers as efficient nanosensor towards toxic HF gas molecules and the PDOS of adsorbed HF gas molecules is also contributed as same as here presented results[63]. Therefore, the remarkable ability of penta-$PdAs_2$ monolayer makes a potential candidate for the H_2S gas sensing applicatons.

Electric transport properties of adsorbed H_2S, HF and H_2 gases on penta-$PdAs_2$ monolayer. To quantitatively probe the gas sensing properties of the $PdAs_2$ being an efficient nano sensor, non-equilibrium *Green's* function formalism (NEGF) was employed to analyze the current (I)-voltage (V) response[64]. The structural schematic model of sensing device set up are shown in Fig. 5. Where, the shaded region shows the elec-

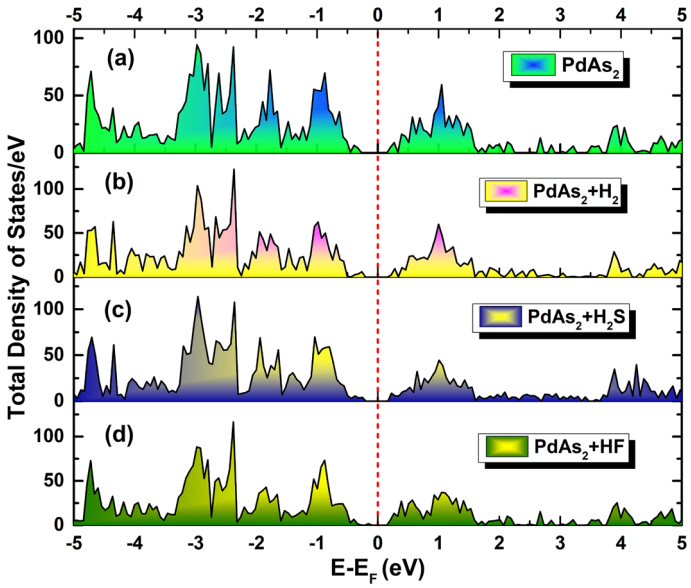

Figure 4. Total density of states/*eV* of (**a**) penta-$PdAs_2$ with adsorbed (**b**) H_2, (**c**) H_2S and (**d**) HF gas molecules.

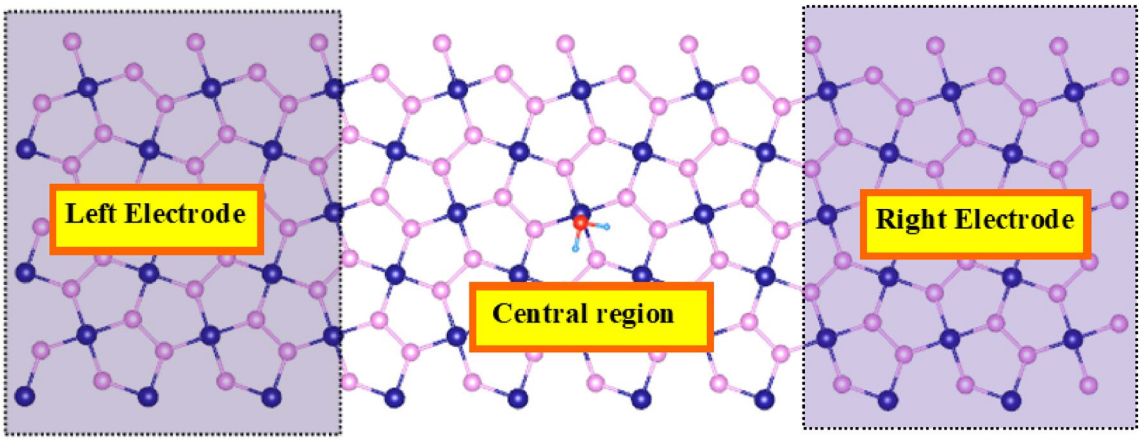

Figure 5. Schematic structural model of a gas sensor based on penta-$PdAs_2 + H_2S$ with two electrodes. The Pd, As, H and S atoms are indicated in navy blue, pink, water blue and red colors, respectively.

trodes which were simulated within the a 3×3 supercell of bare $PdAs_2$ monolayer. The central or scattering region exemplifies the device area, where gas adsorption take place. Figure 6a,b, exhibits the I–V characteristics of $PdAs_2$ before and after gas molecules exposure.

Although the adsorption of H_2S, HF and H_2 gas molecules does not affect much the electronic structure pointedly, but the charge transfer (Q) after their exposure is expected to vary due to doping of electrons or holes during the electron transportation. And these effects are revealed to be possible indication for gas sensors. As shown in Fig. 6b, In the case of bare $PdAs_2$, we found that the current response in the range of micro-ampere (μA). Further, the junction remains switched off at the 0 V but seems switched on with the increasing of bias voltage. Then, noticeably above the 0 V, all the absorbed gas systems have a relevant effect on the transport from the bare one, which making all systems for gas sensing applications.

As seen in Fig. 6a, after the gas exposure the current is reducing from the bare $PdAs_2$ and gives response in order of nA. When bias over 0 V, the current starts to increase simultaneously up to 1.6 V for all cases. Interestingly, after the bias of 1.6 V the current response trends change slightly for all absorbed gas molecules. At V = 1.8 V, the highest current sensitivity (current of 0.32 nA) with current is observed for the $PdAs_2 + H_2S$ system compared to HF and H_2 system. Which could be due to acceptor nature of the H_2S gas molecules. Further, in the H_2 adsorption (Fig. 6a), the current is significantly enhanced and reached up to 0.58 nA at the bias of 2 V. While it calibrate, for H_2S (with current of 0.35 nA) and HF (with current of 0.33 nA) gas exposure a current reduction is about 60% and 56.89%, respectively compared to H_2 gas exposure under the bias of 2 V as summarized in the Table 3. Overall, all the results indicated that the penta-$PdAs_2$ monolayer could be better applicants for achieving the sensitivity and selectivity towards H_2S compare to HF and H_2 gas molecules.

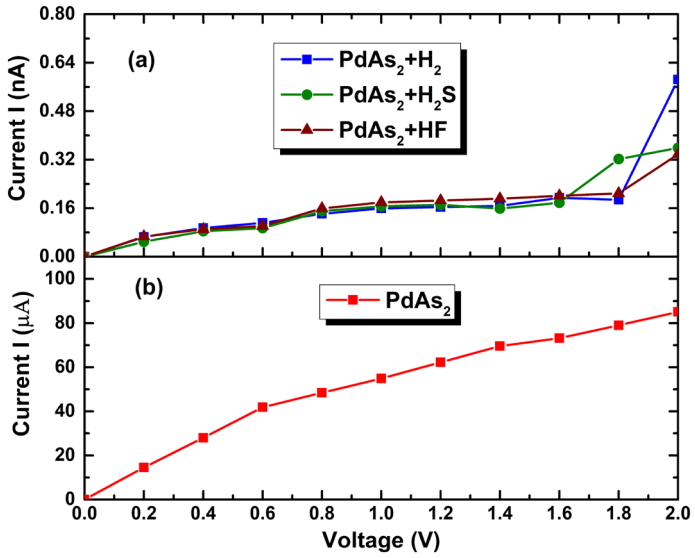

Figure 6. The current–voltage charateristics of adsorbed (**a**) H_2, H_2S and HF gas molecules, (**b**) bare $PdAs_2$ monolayer.

System	Current at bias 2.0 V		Current variation (with adsorbed H_2) (%)
	Current I	Current ratio I_R	
$PdAs_2$ nanosheet	85 μA	1 μA	–
$PdAs_2 + H_2$	0.58 nA	6.82 μA	100
$PdAs_2 + H_2S$	0.35 nA	4.11 μA	60
$PdAs_2$ + HF	0.33 nA	3.88 μA	56.89

Table 3. The current ratio and current variation of H_2, H_2S and HF absorbed $PdAs_2$ nanosheet at the bias voltage of 2.0 V.

Conclusion

In summary, the noxious H_2S, HF and H_2 gas molecules on a penta-$PdAs_2$ nanosheet are first time investigated within the density functional level of theory including van der Waals corrections. We systemically discovered the most favorable binding site of each molecule based on the five different adsorption positions. The adsorption energy (E_{ads}), charge transfer (Q), recovery time (τ) and work function (Φ) were investigated to understand performance and behavior of adsorption of the pollutant on $PdAs_2$ surface. The gas sensitivity order of pollutant gases was predicted as follow: $H_2S > HF > H_2$ on the penta-$PdAs_2$ nanosheet. The obtained recovery time (τ) of the sensor to all target gases are less than 3 min. The adsorption of H_2S and HF results in an obvious increasing in DOS near E_F which is not observed by the adsorption of H_2. Eventually, the *IV* response were carried out to study the responses of bare and absorbed $PdAs_2$ nanosheet and the sharp rises seen at V = 1.8 V in order of $H_2S > HF > H_2$ that shows the authenticated potential as efficient gas sensor. These outcome acclaim the exciting prospects of developing penta-$PdAs_2$ monolayer for the ultrahigh-sensitivity gas sensing nano-devices.

Data availability

The datasets generated and/or analysed during the current study are not publicly available due to privacy or other restrictions. However, it may be made available from the corresponding author on reasonable request.

Received: 11 November 2022; Accepted: 4 January 2023
Published online: 13 January 2023

References

1. Wang, R. Toxic gas, lifesaver. *Sci. Am.* **302**(3), 66–71 (2010).
2. Lim, H., Um, K. & Jung, S. A study on effective mitigation system for accidental toxic gas releases. *J. Loss. Rev. Process Ind.* **49**, 636–644 (2017).
3. Sett, D. & Basak, D. Highly enhanced H2 gas sensing characteristics of Co: ZnO nanorods and its mechanism. *Sen. Actuators B Chem.* **243**, 475–483 (2017).
4. Liu, X. *et al.* A survey on gas sensing technology. *Sensors* **12**(7), 9635–9665 (2012).
5. Hodgkinson, J. & Tatam, R. P. Optical gas sensing: A review. *Meas. Sci. Technol.* **24**(1), 012004 (2012).
6. Feng, S. *et al.* Review on smart gas sensing technology. *Sensors* **19**(17), 3760 (2019).
7. Yamazoe, N. & Miura, N. Environmental gas sensing. *Sens. Actuators B Chem.* **20**(2–3), 95–102 (1994).
8. Verma, R., Vinoda, K. S., Papireddy, M. & Gowda, A. N. S. Toxic pollutants from plastic waste—A review. *Procedia Environ. Sci.* **35**, 701–708 (2016).
9. Kamionka, M., Breuil, P. & Pijolat, C. Calibration of a multivariate gas sensing device for atmospheric pollution measurement. *Sens. Actuators B Chem.* **118**(1–2), 323–327 (2006).
10. Yang, S., Jiang, C. & Wei, S. H. Gas sensing in 2D materials. *Appl. Phys. Rev.* **4**(2), 021304 (2017).
11. Neri, G. Thin 2D: The new dimensionality in gas sensing. *Chemosensors* **5**(3), 21 (2017).
12. Xia, S. Y., Tao, L. Q., Jiang, T., Sun, H. & Li, J. Rh-doped h-BN monolayer as a high sensitivity SF6 decomposed gases sensor: A DFT study. *Appl. Surf. Sci.* **536**, 147965 (2021).
13. Liu, X., Ma, T., Pinna, N. & Zhang, J. Two-dimensional nanostructured materials for gas sensing. *Adv. Funct. Mater.* **27**(37), 1702168 (2017).
14. Cui, H., Zhang, Q., Liu, H. & Peng, X. Janus PtSSe monolayer: A novel strain-modulated buddy for SOF2 sensing. *Vacuum* **198**, 110887 (2022).
15. Mushtaq, M. & Tit, N. Magnetic single atom catalyst in C2N to induce adsorption selectivity toward oxidizing gases. *Sci. Rep.* **11**(1), 1–14 (2021).
16. Ayari, T. *et al.* Gas sensors boosted by two-dimensional h-BN enabled transfer on thin substrate foils: Towards wearable and portable applications. *Sci. Rep.* **7**(1), 1–8 (2017).
17. Habib, I. Y. *et al.* Enhanced carbon monoxide-sensing properties of chromium-doped ZnO nanostructures. *Sci. Rep.* **9**(1), 1–12 (2019).
18. Cho, B. *et al.* Charge-transfer-based gas sensing using atomic-layer MoS2. *Sci. Rep.* **5**(1), 1–6 (2015).
19. Basyooni, M. A., Shaban, M. & El Sayed, A. M. Enhanced gas sensing properties of spin-coated Na-doped ZnO nanostructured films. *Sci. Rep.* **7**(1), 1–12 (2017).
20. Tian, H. *et al.* A graphene-based resistive pressure sensor with record-high sensitivity in a wide pressure range. *Sci. Rep.* **5**(1), 1–6 (2015).
21. Mansouri, E., Karamdel, J., Berahman, M. & Ahmadi, M. T. Phosphorene as H2S and CH4 gas sensor. *Phys. Status Solidi (A)* **216**(2), 1800086 (2019).
22. Sharma, R., Kaur, N., Choudhary, B. C. & Goswamy, J. K. DFT based study of transition metals (Au, Ag, Pd & Pt) doped graphitic carbon nitride (gCN) monolayer as a CO gas sensor. *Phys. Scr.* **97**(6), 065706 (2022).
23. Ahmed, S. *et al.* Ab-initio characterization of B4C3 monolayer as a toxic gases sensing material. *Appl. Surf. Sci.* **544**, 148877 (2021).
24. Cui, H., Zhang, X., Li, Y., Chen, D. & Zhang, Y. First-principles insight into Ni-doped InN monolayer as a noxious gases scavenger. *Appl. Surf. Sci.* **494**, 859–866 (2019).

25. Wang, X. & Wang, J. Effects of Pt and Au adsorption on the gas sensing performance of SnS2 monolayers: A DFT study. *Mater. Sci. Semicond. Process.* **121**, 105416 (2022).
26. Kim, Y. *et al.* Improved sensitivity in Schottky contacted two-dimensional MoS2 gas sensor. *ACS Appl. Mater. Interfaces* **11**(42), 38902–38909 (2019).
27. Panigrahi, P., Hussain, T., Karton, A. & Ahuja, R. Elemental substitution of two-dimensional transition metal dichalcogenides (MoSe2 and MoTe2): Implications for enhanced gas sensing. *ACS Sens.* **4**(10), 2646–2653 (2019).
28. Chen, D. *et al.* Theoretical study of monolayer PtSe2 as outstanding gas sensor to detect SF6 decompositions. *IEEE Electron. Device Lett.* **39**(9), 1405–1408 (2018).
29. Guo, R. *et al.* Ultrasensitive room temperature NO2 sensors based on liquid phase exfoliated WSe2 nanosheets. *Sens. Actuators B Chem.* **300**, 127013 (2019).
30. Bouheddadj, A. *et al.* Low-dimensional HfS2 as SO2 adsorbent and gas sensor: Effect of water and sulfur vacancies. *Phys. Chem. Chem. Phys.* **23**(41), 23655–23666 (2021).
31. Guidotti, T. L. Hydrogen sulphide. *Occup. Med.* **46**(5), 367–371 (1996).
32. Lambert, T. W., Goodwin, V. M., Stefani, D. & Strosher, L. Hydrogen sulfide (H2S) and sour gas effects on the eye. A historical perspective. *Sci. Total Environ.* **367**(1), 1–22 (2006).
33. Schramm, L. L. Fundamentals and applications in the petroleum Industry. *Adv. Chem.* **231**, 3–24 (1992).
34. Rylander, R. Health effects among workers in sewage treatment plants. *Occup. Environ. Med.* **56**(5), 354–357 (1999).
35. Li, L., He, J., Gan, Z. & Yang, P. Occurrence and fate of antibiotics and heavy metals in sewage treatment plants and risk assessment of reclaimed water in Chengdu, China. *Chemosphere* **272**, 129730 (2021).
36. Davis, J. B. & Kirkland, D. W. Bioepigenetic sulfur deposits. *Econ. Geol.* **74**(2), 462–468 (1979).
37. Lim, E., Mbowe, O., Lee, A. S. & Davis, J. Effect of environmental exposure to hydrogen sulfide on central nervous system and respiratory function: A systematic review of human studies. *Int. J. Occup. Environ. Health* **22**(1), 80–90 (2016).
38. Gao, X., Zhou, Q., Wang, J., Xu, L. & Zeng, W. Performance of intrinsic and modified graphene for the adsorption of H2S and CH4: A DFT study. *Nanomaterials* **10**(2), 299 (2020).
39. Bhattacharyya, K., Pratik, S. M. & Datta, A. Controlled pore sizes in monolayer C2N act as ultrasensitive probes for detection of gaseous pollutants (HF, HCN, and H2S). *J. Phys. Chem. C* **122**(4), 2248–2258 (2018).
40. Li, D. *et al.* First-principle insight into the Ru-doped PtSe2 monolayer for detection of H2 and C2H2 in transformer oil. *ACS Omega* **5**(49), 31872–31879 (2020).
41. Pandey, D., Gangwar, R., Bhattacharya, J. & Chakrabarti, A. Study of adsorption of H2, CO and NO gas molecules on molybdenum sulfide and tungsten sulfide monolayers from first-principles calculations. *Surf. Sci.* **714**, 121910 (2021).
42. Shunhong, Z. *et al.* Penta-graphene: A new carbon allotrope. *Proc. Natl. Acad. Sci.* **7**(2), 191–207 (2015).
43. Zhao, K. *et al.* Penta-BCN: A new ternary pentagonal monolayer with intrinsic piezoelectricity. *J. Phys. Chem. Lett.* **11**(9), 3501–3506 (2020).
44. Wei, M., Dou, X., Zhao, L., Du, J. & Jiang, G. Monolayer penta-BCN: A promising candidate for harmful gases detection. *Sens. Actuators A Phys.* **334**, 113326 (2022).
45. Lakhani, K. *et al.* Dissociation of air pollutants on the uniform surface of pentagonal BeP2. *Appl. Surf. Sci.* **570**, 151061 (2021).
46. Xia, X. *et al.* Sensing performance of SO_2, SO_3 and NO_2 gas molecules on 2D pentagonal $PdSe_2$: A first-principle study. *IEEE Electron Device Lett.* **42**(4), 573–576 (2021).
47. Tang, L. *et al.* Ultrahigh sensitivity and selectivity of pentagonal SiC2 monolayer gas sensors: The synergistic effect of composition and structural topology. *Phys. Status Solidi B* **257**(3), 1900445 (2020).
48. Raval, D., Babariya, B., Gupta, S. K., Gajjar, P. N. & Ahuja, R. Ultrahigh carrier mobility and light-harvesting performance of 2D penta-PdX2 monolayer. *J. Mater. Sci.* **56**(5), 3846–3860 (2021).
49. Soler, J. M. *et al.* The SIESTA method for ab initio order-N materials simulation. *J. Phys. Condens. Matter* **14**(11), 2745 (2002).
50. Perdew, J. P., Burke, K. & Ernzerhof, M. Generalized gradient approximation made simple. *Phys. Rev. Lett.* **77**(18), 3865 (1996).
51. Lundqvist, B. I., Andersson, Y., Shao, H., Chan, S. & Langreth, D. C. Density functional theory including van der Waals forces. *Int. J. Quantum Chem.* **56**(4), 247–255 (1995).
52. Chadi, D. J. Special points for Brillouin-zone integrations. *Phys. Rev. B* **16**(4), 1746 (1977).
53. Chen, J., Zhou, Q., Jia, L., Cui, X. & Zeng, W. The gas-sensing mechanism of Pt3 cluster doped SnS2 monolayer for SF6 decomposition: A DFT study. *Appl. Surf. Sci.* **597**, 153693 (2022).
54. Momma, K. & Izumi, F. VESTA: A three-dimensional visualization system for electronic and structural analysis. *J. Appl. Crystallogr.* **41**(3), 653–658 (2008).
55. Truhlar, D. G. & Garrett, B. C. Variational transition-state theory. *Acc. Chem. Res.* **13**(12), 440–448 (1980).
56. Stokbro, K., Taylor, J., Brandbyge, M. & Ordejon, P. TranSIESTA: A spice for molecular electronics. *Ann. N. Y. Acad. Sci.* **1006**(1), 212–226 (2003).
57. Yuan, H., Li, Z. & Yang, J. Atomically thin semiconducting penta-PdP2 and PdAs2 with ultrahigh carrier mobility. *J. Mater. Chem. C* **6**(34), 9055–9059 (2018).
58. Majidi, R. & Ramazani, A. Detection of HF and H2S with pristine and Ti-embedded twin graphene: A density functional theory study. *J. Phys. Chem. Solids* **132**, 31–37 (2019).
59. Cai, Y., Ke, Q., Zhang, G. & Zhang, Y. W. Energetics, charge transfer, and magnetism of small molecules physisorbed on phosphorene. *J. Phys. Chem. C* **119**(6), 3102–3110 (2015).
60. Freeouf, J. L. & Woodall, J. M. Schottky barriers: An effective work function model. *Appl. Phys. Lett.* **39**(9), 727–729 (1981).
61. Yu, Y. J. *et al.* Tuning the graphene work function by electric field effect. *Nano Lett.* **9**(10), 3430–3434 (2009).
62. Opoku, F. & Govender, P. P. Two-dimensional CoOOH as a highly sensitive and selective H2S, HCN and HF gas sensor: A computational investigation. *Electroanalysis* **32**(12), 2764–2774 (2020).
63. Pal Kaur, S., Hussain, T. & Dhilip Kumar, T. J. Substituted 2D Janus WSSe monolayers as efficient nanosensor toward toxic gases. *J. Appl. Phys.* **130**(1), 014501 (2021).
64. Brandbyge, M., Mozos, J. L., Ordejón, P., Taylor, J. & Stokbro, K. Density-functional method for nonequilibrium electron transport. *Phys. Rev. B* **65**(16), 165401 (2002).

Acknowledgements

The computer facility developed under DST-FIST Level-I (No. SR/FST/PSI-097/2006 dated 20th December 2006 and No. SR/FST/PSI-198/2014 dated 21 November 2014) programmes of Department of Science and Technology, Government of India, New Delhi, India and support under DRS-SAP-I (No. F-530/10/DRS/2010 (SAP-I) dated November 2010 and No. F.530/17/DRS-II/2018 (SAP-I), dated 17th April 2018) of University Grants Commission, New Delhi, India are highly acknowledged. DR is thankful for the project fellowship under DRS-II-SAP (No.F.530/17/DRS-II/2018 (SAP-I), dated 17/04/2018) of University Grants Commission, New Delhi, India. S.K.G. would like to thank the Science and Engineering Research Board (SERB), India for the financial support (Grant No.: YSS/2015/001269).

Author contributions

D.R., S.K.G. and P.N.G. studied the conception and designed the final approval of the version to be published. D.R. was associated with the DFT calculations. S.K.G., and P.N.G. contributed to the improvement of the scientific content of the article. All authors reviewed the manuscript.

Competing interests

The authors declare no competing interests.

Additional information

Supplementary Information The online version contains supplementary material available at https://doi.org/10.1038/s41598-023-27563-x.

Correspondence and requests for materials should be addressed to S.K.G. or P.N.G.

Reprints and permissions information is available at www.nature.com/reprints.

Publisher's note Springer Nature remains neutral with regard to jurisdictional claims in published maps and institutional affiliations.